

Diff-Aid: Inference-time Adaptive Interaction Denoising for Rectified Text-to-Image Generation

Binglei Li^{1,2} Mengping Yang^{1,3†} Zhiyu Tan^{1,3} Junping Zhang^{1,‡} Hao Li^{1,2,3,§}

† Project Lead § Corresponding Authors

{b1li24}@m.fudan.edu.cn, {jpzhang, lihao_lh}@fudan.edu.cn

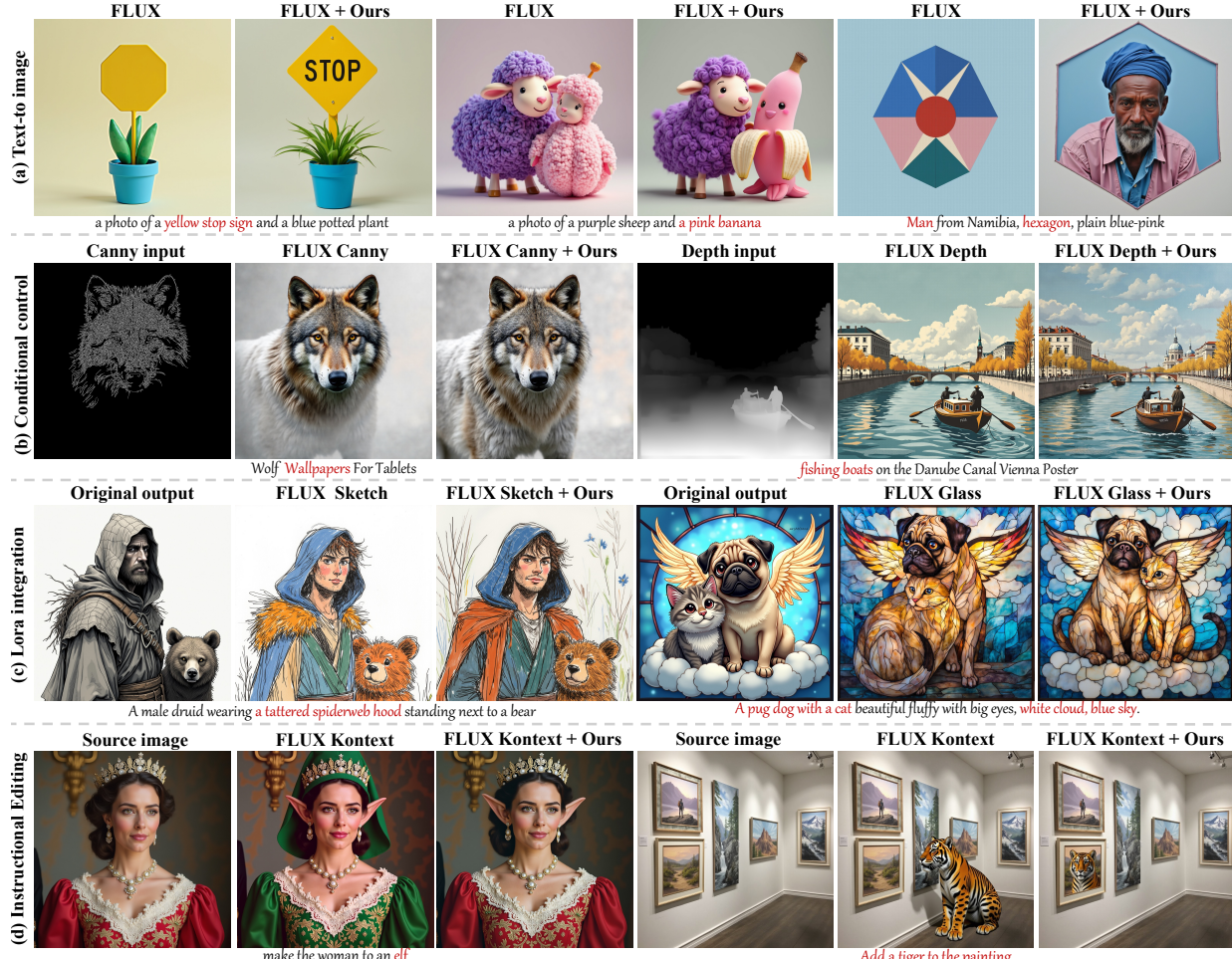


Figure 1. We present **Diff-Aid** to adaptively improve the interaction between textual conditions and image latents during test time. Benefited from our *plug-in* design, **Diff-Aid** enables improved prompts following and synthesis quality for (a) Text-to-image generation, (b) adding conditional input for controllable generation, (c) integrating off-the-shelf LoRAs and (d) zero-shot instructional image editing.

Abstract

Recent text-to-image (T2I) diffusion models have achieved remarkable advancement, yet faithfully following complex textual descriptions remains challenging due to insufficient interactions be-

¹Fudan University ²Shanghai Innovation Institute ³Shanghai Academy of AI for Science, [†]Project Lead. Correspondence to: Hao Li <lihao_lh@fudan.edu.cn>, Junping Zhang <jpzhang@fudan.edu.cn>.

tween textual and visual features. Prior approaches enhance such interactions via architectural design or handcrafted textual condition weighting, but lack flexibility and overlook the dynamic interactions across different blocks and denoising stages. To provide a more flexible and efficient solution to this problem, we propose **Diff-Aid**, a lightweight inference-time method that adaptively adjusts per-token text and image interactions across transformer blocks and denoising timesteps. Beyond improving generation quality,

Diff-Aid yields interpretable modulation patterns that reveal how different blocks, timesteps, and textual tokens contribute to semantic alignment during denoising. As a plug-and-play module, *Diff-Aid* can be seamlessly integrated into downstream applications for further improvement, including style LoRAs, controllable generation, and zero-shot editing. Experiments on strong baselines (SD 3.5 and FLUX) demonstrate consistent improvements in prompt adherence, visual quality, and human preference across various metrics. Our code and models will be released.

1. Introduction

Diffusion models (DMs) (Ho et al., 2020; Song et al., 2021), which iteratively denoises random noisy samples into high-quality outputs, have revolutionized the experiences of AI generated content (AIGC) in various applications including text-to-image (Ma et al., 2024; Esser et al., 2024), text-to-video generation (Yang et al., 2025; Team, 2024a; OpenAI, 2024; Wan et al., 2025), joint audio-video synthesis (Wang et al., 2026; Zhang et al., 2025), etc. These breakthroughs mainly stem from the scalability of diffusion transformers (DiT) (Peebles & Xie, 2023; Liu et al., 2023) over conventional U-Net models (Rombach et al., 2022; Dhariwal & Nichol, 2021), as well as advances in large-scale training compute, infra and data pipelines. Yet, considering DMs as a model that maps textual conditions to visual outputs, they might often fail to produce images that accurately reflect textual details due to insufficient interactions between textual conditions and image features. For instance, the current top-performing model FLUX (Labs, 2024) failed to produce the “yellow stop sign” in Fig. 1 (a).

Many prior approaches have been developed to strengthen cross-modal interactions between text and image representations. On the architecture design hand, early methods rely on cross-attention mechanisms to inject textual information into diffusion models (Rombach et al., 2022; Team, 2024b), while Peebles & Xie (2023) proposed adaLN-zero strategy to condition transformer blocks on class conditions. The most recent multimodal diffusion transformers (MMDiT) based approaches (Labs, 2024; Stability-AI, 2024; Wu et al., 2025) employ a shared unified transformer to jointly model both modalities, facilitating cross-modal interactions. However, training such models from scratch requires massive compute and data. On the other hand, classifier-free guidance (CFG) (Ho & Salimans, 2022) adopts a static scaling factor to balance conditional and unconditional model outputs, thus improving conditioning strength. TACA (Lv et al., 2025) pointed out that semantic discrepancies may arise from the suppression of cross-modal attention due to the numerical asymmetry between the number of visual

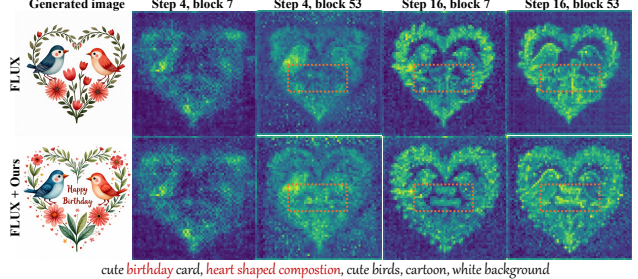


Figure 2. Attention visualization of different blocks across denoising steps. If the interaction between textual conditions and image latents is insufficient, the rendered image may fail to faithfully reflect given conditions.

and text tokens and proposed a handcrafted weighting strategy to enhance textual tokens. Further, Li et al. (2026) probed specific roles of transformer blocks in rendering textual conditions and attached block-specific enhancements to improve interactions. Yet, they require heuristic search of weighting strategies across the forward process, without explicitly considering the dynamic interactions between textual and visual features throughout the denoising process.

In this paper, we aim to develop a lightweight, plug-in, and adaptive method to dynamically adjust interactions between textual and visual features during inference time, thereby delivering high-quality output images with improved prompt following and human preferences. As shown in Fig. 2, we notice that 1) certain transformer blocks exhibit distinct patterns of text-image interaction at different denoising steps, and 2) the interaction between textual conditions and image features determines the content of generated images. That is, the rendered image would be sub-optimal if the interaction is insufficient. Additionally, it is intuitive that different textual tokens might contribute differently to the final image, while there are no prior attempts assigned token-specific importance based on their contributions. Consequently, we hypothesize that learning adaptive importance weights for textual tokens across blocks and timesteps is key to improving semantic alignment and generation quality.

Capitalizing on the above observations, we propose *Diff-Aid*, an inference-time Adaptive Interaction Denoising paradigm for text-to-image DiT models. Concretely, *Diff-Aid* introduces two key innovations: 1) an *Aid* module, which explicitly adjusts textual conditions according to the varied blocks, timesteps, and tokens; and 2) a gated sparsity and stabilized regularization mechanism that respectively ensure attaching more attention to important blocks and avoiding training collapse. In this way, the learned parameters for adjustment are interpretable with respect to different blocks, varied timesteps, and textual tokens, further providing insights into the model’s internal behavior (as illustrated in Fig. 4). More importantly, our design is lightweight with a small number of trainable parameters, without modifying the representation space of pretrained models. As illustrated in Fig. 1,

as a plug-in module, *Diff-Aid* can be seamlessly integrated into homologous models for controllable image generation (b), styled LoRA generation (c), and instructional image editing (d), demonstrating its versatility and effectiveness. We evaluate our *Diff-Aid* on two strong baseline models (*i.e.*, SD 3.5 (Esser et al., 2024) and FLUX (Labs, 2024)), the consistent performance improvements across varied metrics and benchmarks demonstrate the effectiveness of our design. Further analysis reveals that *Diff-Aid* learns meaningful and interpretable interaction patterns aligned with the denoising dynamics, validating our design principles.

To sum up, our contributions are: 1) We propose *Diff-Aid*, a lightweight model to adaptively manipulate the interactions between textual and visual features at inference-time, capturing the dynamic relationships across different blocks, timesteps, textual tokens, as well as the intrinsic properties of baseline models. 2) Our *Diff-Aid* is designed as a plug-in and generalizable module that can be seamlessly integrated for downstream applications, including LoRAs, controllable generation, and zero-shot image editing. 3) Extensive experiments across multiple baseline models and evaluation metrics demonstrate consistent improvements in prompt following, visual quality, and human preferences.

2. Methodology

2.1. Systematic Analysis of Design Motivations

Interactions between textual conditions and image latents for T2I. Text is the primary guidance for image generation in text-to-image diffusion models. The diffusion model is indeed a mapper $\mathcal{F} : \mathcal{P}_{txt} \rightarrow \mathcal{X}_{img}$, where the prompt is the only condition to generate the image. MMDiT models (Esser et al., 2024; Labs, 2024) leverage joint self-attention to integrate text and image features:

$$\begin{aligned} \mathbf{z}_t^{l+1} &= \text{Softmax} \left(\mathbf{Q} \mathbf{K}^T / \sqrt{d} \right) \mathbf{V} + \mathbf{z}_t^l; \\ [\mathbf{Q}, \mathbf{K}, \mathbf{V}] &= W_{qkv} \cdot \text{LN}([\mathbf{z}_t^l, \mathbf{c}_t^l]). \end{aligned} \quad (1)$$

Therefore, effective interaction in attention between textual and visual tokens is vitally important for high-quality image generation. For example, Fig. 2 shows two denoising trajectories of the same prompt and initial noise but different text-image interaction patterns. The attention maps of the second trajectory, highlighted in red boxes, have a stronger focus on the relevant text token “birthday”, leading to better text-image alignment.

Principle 1: Cross-modal interaction matters

Attention mechanism enables text-image interaction, which is crucial for high-quality image generation in Diffusion models.

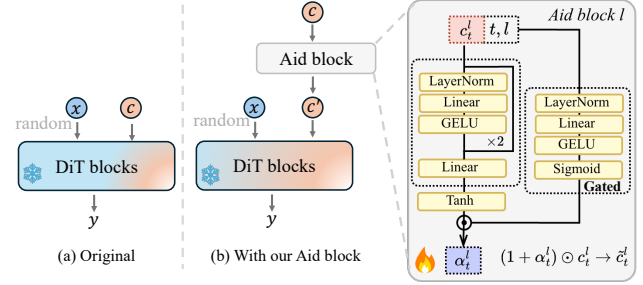


Figure 3. Overview of our proposed Aid blocks. (a) The original diffusion transformers map a random latent and input textual conditions to output features. (b) Our Aid blocks adaptively modulate textual conditions with respect to denoising timesteps across different transformer blocks, enhancing the interaction between image latents and textual conditions.

Sufficient interactions lead to improved prompt adherence. **Sufficient interactions lead to improved prompt adherence.** Attention within each transformer block facilitates the integration of text and image features. As shown in Fig. 2 (second row), different blocks exhibit different patterns, where the 7th block focuses more on structure while the 53rd block emphasizes the “birthday” token. Therefore, we should consider a block-specific architecture to adaptively modulate interactions to leverage the unique capabilities of each block. Moreover, the denoising process in DiTs is indeed a PF-ODE solving procedure (Liu et al., 2023), where different timesteps contribute different guidance strengths from text features. Actually, Fig. 4(d) shows that attention norms differ across timesteps and different blocks. Thus, timestep-aware modulation is also necessary to manage the interaction strength dynamically. To mitigate the problem of imbalanced visual and textual tokens ($N_x \gg N_c$) (Lv et al., 2025), we introduce a token-level modulation mechanism for text features with different lengths. All these observations motivate our designs.

Principle 2: per-token interaction across blocks and timesteps

Modulating text features at block-specific, timestep-aware, and token-level dimensions is essential and effective for enhancing text-image interactions.

2.2. The Proposed *Diff-Aid*

Adaptive interaction denoising (AiD) module. We propose *Aid* ϕ that learns the coefficient $\alpha_t^l \in \mathbb{R}^N$ to modulate text-image interactions based on the current diffusion timestep, transformer block, and text features.

$$\alpha_t^l = \phi(\mathbf{c}_t^l, t, l), \quad \alpha_t^l \in [-1, 1]^N, \quad (2)$$

where \mathbf{c}_t^l represents the text features at timestep t and transformer block l , N is the number of text tokens. Then, we modulate the text features as:

$$\tilde{\mathbf{c}}_t^l = \mathbf{c}_t^l + \mathbf{c}_t^l \odot \alpha_t^l, \quad (3)$$

where \odot is element-wise multiplication. The modulated $\tilde{\mathbf{c}}_t^l$ is the input for the next block. The *Aid* ϕ is implemented as a lightweight multi-layer perceptron with a gated mechanism and bounded activation functions (*i.e.*, tanh) to ensure stability and effective modulation, as shown in Fig. 3.

Improving distribution sparsity across blocks. We expect the learned α_t^l to be sparse for two main reasons. 1) Not all text tokens are equally important; some tokens carry more semantic information than others. For example, max sequence lengths of text tokens are 512 in FLUX and 333 in SD 3.5, but most prompts contain only approximately $50 \sim 200$ tokens, and the rest are often less informative, such as “PAD” tokens. 2) Not all transformer blocks require strong text conditioning. Commonsense from previous works (Alaluf et al., 2024; Li et al., 2026) indicates that early blocks focus more on semantic and structural information, while later blocks refine visual details. Therefore, the α_t^l should be sparse, allowing the model to focus on the most relevant tokens and transformer blocks.

To achieve this, we facilitate two strategies. First, we introduce a regularization term on the modulation coefficients, which penalizes large values of α_t^l :

$$\mathcal{L}_{reg} = \mathbb{E}_{t,l} [\|\alpha_t^l\|_2]. \quad (4)$$

Second, inspired by Qiu et al. (2025), we apply a gated mechanism in *Aid* to promote sparsity:

$$\alpha_t^l = \phi(\mathbf{c}_t^l, t, l) = \tanh(\mathbf{c}_t^l W_l) \cdot \sigma(\mathbf{c}_t^l W_g), \quad (5)$$

where W_l is the feature weights, and W_g is the gating weights. The gate score $\sigma(\mathbf{c}_t^l W_g)$ effectively acts as a dynamic filter, controlling the strength of the text features by selectively allowing or blocking the modulation signal. These strategies help the *Aid* learn implicit and efficient α to enable block-specific and token-level modulation.

Optimization choices. *Aid* modules are trained using the standard diffusion loss, which minimizes the squared error between the predicted velocity and the target velocity:

$$\mathcal{L}_{diff} = \mathbb{E}_{t,\epsilon,\mathbf{x}} [\|v_\theta(\mathbf{z}_t, t, \tilde{\mathbf{c}}_t) - (\epsilon - \mathbf{x})\|_2^2], \quad (6)$$

where v_θ is the velocity predicted by the diffusion model. To further enhance text-image alignment, we also incorporate the Direct Preference Optimization (DPO) loss (Wallace et al., 2024). DPO optimizes the model based on human preference data, making the model’s outputs more aligned with human judgments:

$$\begin{aligned} \mathcal{L}_{dpo} &= -\mathbb{E}_{(\mathbf{x}^+, \mathbf{x}^-), t} \left[\log \sigma \left(\beta (\Delta s_\theta - \Delta s_{ref}) \right) \right], \\ \Delta s_\theta &= s_\theta(\mathbf{z}_t^+, t, \tilde{\mathbf{c}}_t^+) - s_\theta(\mathbf{z}_t^-, t, \tilde{\mathbf{c}}_t^-), \\ \Delta s_{ref} &= s_{ref}(\mathbf{z}_t^+, t, \tilde{\mathbf{c}}_t^+) - s_{ref}(\mathbf{z}_t^-, t, \tilde{\mathbf{c}}_t^-), \end{aligned} \quad (7)$$

where $(\mathbf{x}^+, \mathbf{x}^-)$ are pairs of preferred images, σ is the sigmoid function, and β is the scaling factor. s_θ and s_{ref} denote score functions of the current and the reference model, respectively. To make the optimization more stable and α_t^l

more robust, we randomly skip the *Aid* modules during training with a probability of p . This mutes the entire *Aid* rather than individual neurons, akin to dropout.

Differences between our *Diff-Aid* and existing approaches. LoRA introduces low-rank updates to transformer weights, which is an efficient fine-tuning strategy. Controlnet adds additional networks to provide extra conditions, which are usually layout or structure information. They do not explicitly address the dynamic nature of text-image interactions in diffusion transformers. One similar approach is CFG (Ho & Salimans, 2022), which statically scales the conditional and unconditional model outputs. However, our approach modulates before the attention mechanism and provides fine-grained, adaptive modulation per-token across transformer blocks and timesteps.

2.3. Training and Inference

During training, we freeze the backbone MMDiT model and only optimize the *Aid* ϕ using the combined loss:

$$\mathcal{L} = \mathcal{L}_{diff} + \lambda_{dpo} \mathcal{L}_{dpo} + \lambda_{reg} \mathcal{L}_{reg}, \quad (8)$$

where λ_{dpo} and λ_{reg} are hyperparameters. During inference, the lightweight *Aid* modules are all active and inserted into each transformer block. Other than the integration of our proposed *Aid*, the inference process remains unchanged. Regarding downstream applications such as LoRAs and editing, our weights are directly loaded for zero-shot inference.

3. Experiments

3.1. Experiment Settings

Implementation details. We adopt FLUX.1-Dev (Labs, 2024) and SD3.5-Large (Stability-AI, 2024) as baselines. During training, we freeze all backbone parameters and only optimize the *Aid* modules. For optimization, we use the Prodigy optimizer (Mishchenko & Defazio, 2024) with a learning rate of 1.0 and gradient accumulation of 16, yielding an effective batch size of 256. The factor β is set to 0.1. Training runs for 1,000 steps (3.3 epochs) on 8 H100 GPUs (approximately 6 hours for FLUX and 4.5 hours for SD 3.5). We set the dropout probability $p = 0.1$, $\lambda_{dpo} = 1.0$, and $\lambda_{reg} = 0.1$. During inference, all the *Aid* modules are activated. We sample 1024×1024 images using the EDM (Karras et al., 2022) sampler for 28 steps, with CFG scales of 3.5 (SD3.5) and 7.0 (FLUX).

Datasets and evaluation metrics. We train on a subset of HPDv3 (Ma et al., 2025), which are filtered by high preference confidence scores and image quality. We evaluate *Diff-Aid* on the full HPDv3 benchmark for image quality and human preference alignment, as well as GenEval (Ghosh et al., 2023) for semantic understanding. In addition, we assess the generalizability of *Diff-Aid* using out-of-distribution

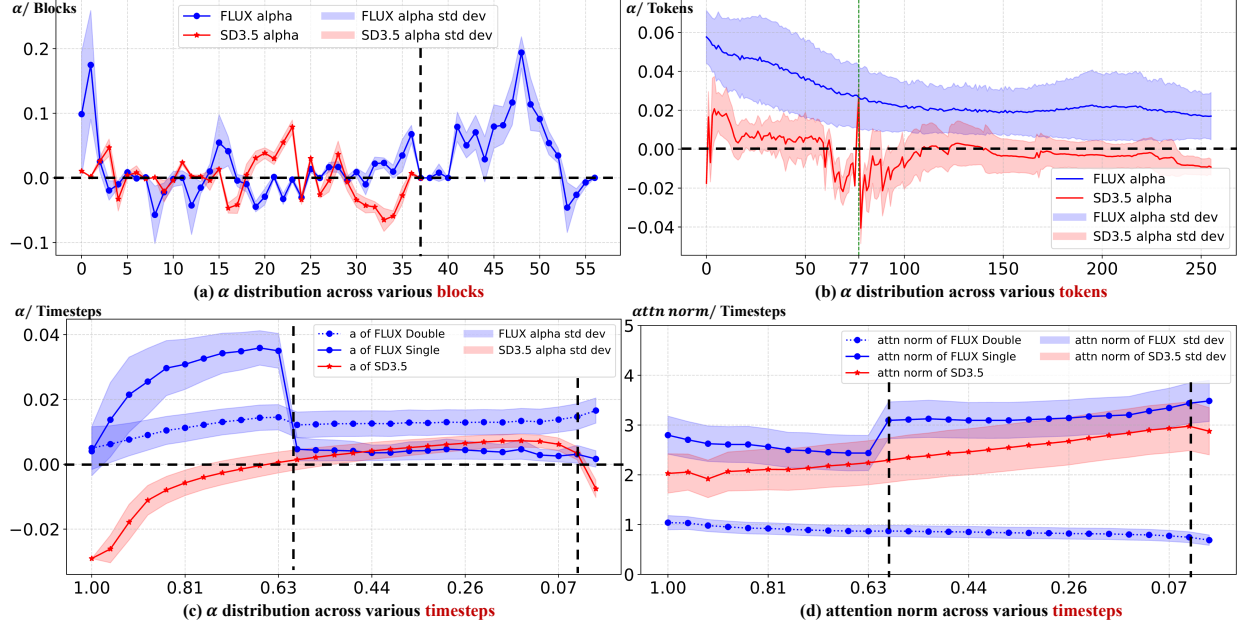


Figure 4. Distributional visualization of the learned adaptive weights α across various (a) diffusion transformer blocks, (b) textual tokens and (c) denoising timesteps. (d) Visualization of the attention norm across various timesteps. Our *Diff-Aid* learns to adaptively adjust block-wise interactions between token-level textual conditions across denoising trajectories, while also capturing the intrinsic attributes of the baseline models to enable tighter and more faithful conditioning during generation.

metrics such as HPSv2 (Wu et al., 2023), ImageReward (Xu et al., 2023) and Aesthetic Score (Schuhmann, 2022). Regarding the zero-shot editing task, we utilize EditBench (Lin et al., 2024) for quantitative assessment.

3.2. Empirical Observation of Learned α

To verify that our *Diff-Aid* learns to adaptively adjust block-wise interactions between token-level textual conditions across denoising trajectories, we analyze the learned coefficients $\alpha_t^l \in \mathbb{R}^N$ cached in each *Aid* block during denoising. Fig. 4 visualizes the distributions of α across different dimensions and the attention norm across various timesteps based on our *Diff-Aid* applied to FLUX and SD 3.5.

α adaptively exhibits sparse and independent patterns across different transformer blocks. The distribution of α across various blocks is shown in Fig. 4(a). We could observe that the former blocks (1st – 3rd in FLUX and 2nd – 4th in SD 3.5) and the latter blocks (41st – 52nd in FLUX and 30th – 35th in SD 3.5) exhibit larger α values than the middle blocks. This aligns well with the observations (Hertz et al., 2022; Cao et al., 2023; Li et al., 2026) that early blocks focus on coarse structure and late blocks refine fine details. Additionally, there are noticeable zero regions in several blocks, showing the effectiveness of our sparsity strategies. The α learned by *Diff-Aid* effectively captures the varying importance of different transformer blocks in text-image interactions.

α assigns token-specific importance weights to different

textual tokens. The α distribution across token positions is shown in Fig. 4(b). The vertical line indicates the boundary between two concatenated text encoders in SD 3.5. In total, α shows a declining trend as token position increases for both models. This is expected since earlier tokens typically carry more semantic weight in prompts, while later tokens often include less informative padding or filler words. Notably, the abrupt change around token index 77 in SD 3.5 coincides with the two text encoders’ boundary. All these observations confirm that our *Diff-Aid* accurately captures token-level importance variations.

α implicitly learns dynamic timestep awareness throughout denoising trajectories. To investigate the timestep-awareness of α , we visualize its distribution throughout the denoising process in Fig. 4(c). Each block’s α values are shown in Fig. 10a and Fig. 10b of appendix. FLUX is split into two parts due to its single-stream and dual-stream architectures. The different types of blocks behave differently, while single-stream blocks show a clear drop in α values at $t = 0.607$, while the dual-stream blocks and SD 3.5 blocks exhibit smooth changes. Such trend indicates that *Diff-Aid* implicitly learns to adjust text-image interactions dynamically across timesteps.

α aligns the intrinsic attributes of pretrained models for efficient and effective adaptation. To explain the α changes across denoising trajectories, we visualize the attention norm of textual and image features in attention blocks across timesteps in Fig. 4(d). We could clearly observe that



Figure 5. Qualitative comparisons of images generated by baseline FLUX and SD 3.5 with and without our proposed Diff-Aid. The quantitative results below each image shows the scores of HPSv3, Image Reward and Aesthetic. Our method demonstrates superior prompt adherence and image quality. More qualitative results are given in appendix.

the dashed vertical lines in Fig. 4(d) perfectly align with the sharp changes in α in Fig. 4(c). Based on the observations, our learned α already captures the intrinsic attribute changes of pretrained models across timesteps, enabling efficient and effective adaptation for the text-image interactions.

3.3. Main Results

Qualitative results. To demonstrate the effectiveness of our proposed *Diff-Aid*, we present qualitative comparisons of images generated by different models given the same prompts and seeds in Fig. 1 and Fig. 5. FLUX with *Diff-Aid* accurately captures the “Nailpolish” and “Male”, generates a correct quantity of “donuts” and “sneaker with tank wheels”. SD 3.5 with *Diff-Aid* effectively synthesizes the “christmas frog” and “rabbit wedding” with semantic details and better visual quality. Although derived from the same noise, *Diff-Aid* adaptively denoises to better trajectories according to the prompts, demonstrating its effectiveness in enhancing prompt adherence and image quality.

Quantitative results on HPSv3 benchmark. We conduct quantitative comparisons on the HPSv3 benchmark (Ma et al., 2025). The results are summarized in Tab. 1. Both FLUX and SD 3.5 benefit from our *Diff-Aid*, with improvements of 0.29 and 0.17 in overall HPSv3 score, compared to their respective baselines. Our method also competes favorably against TACA (Lv et al., 2025), and FLUX combined with *Diff-Aid* even outperforms current SoTA Kolors (Team, 2024b) in overall score and most categories. These significant improvements across all categories validate *Diff-Aid*’s capability towards diverse and complex prompts, leading to improved human preferences.

Generalization to other metrics and benchmark. Al-

though *Diff-Aid* is optimized solely on the HPDV3 dataset, it brings consistent improvements on widely-used metrics such as HPSv2, ImageReward, and Aesthetic Score. The results are summarized in Tab. 2. HPSv2 scores improve by 0.15 and 0.20 for SD 3.5 and FLUX when combined with *Diff-Aid*, respectively. Moreover, *Diff-Aid* also improves the GenEval performance, achieving 5% and 2% improvements for SD 3.5 and FLUX, respectively. These results validate the effectiveness and generalizability of our approach across different evaluation metrics and benchmarks.

3.4. Ablation Studies

To identify the efficacy of each component and optimization choice in our *Diff-Aid*, here we perform ablation studies by disabling each component for evaluation. Specifically, we train various variants on the FLUX baseline following the same settings in Sec. 3 except specific component is removed. We calculate quantitative scores on a random 20% subset of HPDV3 benchmark for a more efficient investigation. The quantitative results are presented in Tab. 3.

Ablation on boundedness and sparsity constraints. Recall that we introduce a regularization term and a gated mechanism to respectively stabilize and sparsify the values of α in Sec. 2. The results in Tab. 3 show that the performance degrades when these constraints are removed. Compared to simply clipping the α values, using Tanh activation yields better results(10.61 vs. 7.12 on HPSv3). Adding a smaller regularization weight ($\lambda_{reg} = 0.1$) further improves the performance than a larger one ($\lambda_{reg} = 1.0$). Armed with the gated mechanism, the model achieves the best results (28.71 on HPSv2, 10.74 on HPSv3) compared to the following settings. Ablation studies validate the effectiveness of our proposed boundedness and sparsity constraints

Table 1. Quantitative comparisons of strong baselines and our proposed *Diff-Aid* on the HPSv3 benchmark. *Diff-Aid* significantly improves the baseline models across categories and even outperforms the current leading Kolors in most categories when applied to FLUX. [†] denotes results evaluated by ourself and ^{*} scores are quoted from the official HPSv3 leaderboard (Ma et al., 2025). **Bold** and underline indicate the best and second-best results, respectively.

Models	All	Char.	Arts	Design	Archi.	Animals	Scenery	Transpor.	Products	Plants	Food	Science	Others
Kolors (Team, 2024b) [*]	<u>10.55</u>	11.79	10.47	9.87	10.82	<u>10.60</u>	9.89	10.68	<u>10.93</u>	<u>10.50</u>	10.63	<u>11.06</u>	9.51
FLUX (Labs, 2024) [*]	10.43	11.70	10.32	9.39	10.93	10.38	10.01	10.84	11.24	10.21	10.38	11.24	9.16
Infinity (Han et al., 2025) [*]	10.26	11.17	9.95	9.43	10.36	9.27	<u>10.11</u>	10.36	10.59	10.08	10.30	10.59	9.62
SD 3 (Esser et al., 2024) [*]	5.31	6.70	5.98	5.15	5.25	4.09	5.24	4.25	5.71	5.84	6.01	5.71	4.58
SD 3.5 [†]	9.31	9.66	8.63	8.58	10.03	8.81	8.90	9.58	9.67	9.78	10.05	8.60	9.46
SD 3.5 + TACA [†]	9.44	9.81	8.82	8.54	10.31	8.92	9.26	9.54	9.96	9.85	10.05	8.81	9.48
SD 3.5 + Ours	9.48	9.93	8.87	8.69	10.22	9.00	9.17	9.80	9.76	9.87	10.18	8.74	9.55
FLUX [†]	10.42	11.67	10.31	9.35	10.94	10.37	9.97	10.87	10.48	10.39	11.20	9.24	10.24
FLUX + TACA [†]	10.48	11.72	10.35	9.36	<u>10.97</u>	10.45	10.03	<u>11.04</u>	10.53	10.46	11.20	9.33	<u>10.35</u>
FLUX + Ours	10.71	11.96	10.72	9.90	<u>11.19</u>	10.62	10.18	11.24	10.61	10.67	<u>11.18</u>	9.68	10.58

Table 2. Quantitative comparisons of more image quality metrics. Despite trained only on HPDV3 dataset, our proposed *Diff-Aid* generalizes to other metrics and gains consistent improvements on these metrics. Note that GenEval scores are computed from official GenEval benchmarks.

Models	HPSv2	HPSv3	ImgRwd	Aes.	GenEval
SD 3.5	<u>28.86</u>	9.31	<u>0.94</u>	6.42	0.72
SD 3.5 + TACA	28.89	<u>9.44</u>	0.93	6.44	<u>0.73</u>
SD 3.5 + Ours	29.01	9.48	1.05	6.53	0.77
FLUX	28.53	10.42	0.89	6.65	0.68
FLUX + TACA	28.59	<u>10.48</u>	0.90	<u>6.68</u>	0.68
FLUX + Ours	28.73	10.71	<u>0.94</u>	6.73	0.70

in stabilizing and enhancing the learning of α .

Ablation on optimization choices and Aid skip probability. We also investigate the impact of different optimization strategies in Sec. 2.2. LORA-based methods yield marginal improvements over the FLUX baseline. In contrast, our *Aid* modules combined with either reward optimization or DPO significantly boost performance. By ablating dropout probabilities p during training, we find that *Aid* with DPO and a small $p = 0.1$ achieves the best results across all metrics.

3.5. Generalized Downstream Applications

Generalizing to zero-shot instruction-based editing. Our *Aid* blocks can be directly inserted into FLUX.1 Kontext (Black Forest Labs et al., 2025) without any additional training. We evaluate the edited images on the EditBench benchmark (Lin et al., 2024), as summarized in Tab. 4. All the metrics show consistent improvements when *Diff-Aid* is applied to Kontext. Notably, CLIP-I and CLIP-T scores increase by 0.93 and 0.06, respectively, indicating better alignment with editing instructions. Visualizations in Fig. 1 and Fig. 6 further keep the original details while accurately following editing instructions.

Integrating with conditional control models. Cooperating with ControlNet (Zhang et al., 2023), our *Diff-Aid* can

Table 3. Ablation study on key components of our proposed method, namely boundedness constraints, sparsity constraints, and optimization strategies. The metrics are computed on the 20% subset of HPDV3 benchmark under the same evaluation settings. “+” means adding the new component on the previous setting. The *italicized* settings are our default choices.

Categories	Settings	HPSv2	HPSv3	ImgRwd	Aes.
FLUX	-	28.53	10.42	0.89	6.66
Bounded Constraints	No Const.	20.03	6.41	-2.04	3.54
	+ Clip	22.86	7.12	0.31	4.07
	+ <i>Tanh Act</i>	28.63	10.61	0.92	6.68
Sparsity Constraints	+ Reg(1.0)	28.49	10.44	0.90	6.64
	+ <i>Reg</i> (0.1)	28.56	10.50	0.90	6.68
	+ <i>Gated</i>	28.71	10.74	<u>0.94</u>	6.72
Drop p	+ drop(0.5)	28.21	10.19	0.77	6.59
	+ drop(0.3)	28.47	10.44	0.87	6.64
	+ drop(0.1)	28.80	10.84	0.95	6.76
Optimization Choices	LoRA + SFT	28.54	10.43	0.86	6.63
	LoRA + DPO	28.57	10.48	0.90	6.67
	Ours + Rwd	<u>28.76</u>	<u>10.78</u>	0.93	<u>6.73</u>
	<i>Ours</i> + DPO	28.80	10.84	0.95	6.76

further enhance controllable generation by improving the interactions between complex textual conditions. In Fig. 1 and Fig. 7, our method effectively captures the semantic details, such as the “*Wolf*” and “*chasing a ball*”, which are missed by the baseline. Moreover, “*one yellow*” stop sign is accurately generated with *Diff-Aid*, showing its effectiveness in handling complex textual conditions.

Combining with existing LoRAs. When combined with LoRAs from the community, our *Diff-Aid* boosts the generation quality while preserving the desired styles. In Fig. 1 and Fig. 8, the images generated by combining *Diff-Aid* exhibit richer details and more vivid textures.

4. Related Works

Diffusion transformers. DiT (Peebles & Xie, 2023) pioneers the use of transformers (Vaswani et al., 2017) in

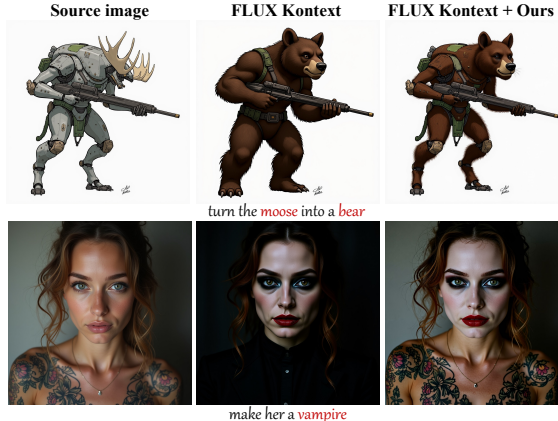


Figure 6. Qualitative results of generalizing *Diff-Aid* to instructional image editing. Although not specifically trained for this task, our methods contribute to improved editing instruction understanding and identity preservation.

Table 4. Quantitative comparison of instructional image editing tasks on EditBench benchmark. Despite trained on the pure text-to-image setting of FLUX, our *Diff-Aid* generalizes to homologous Kontext by enhancing test-time interactions between editing prompts and images in a zero-shot manner.

Models	HPSv2	HPSv3	ImgRwd	Aes.	CLIP-I	CLIP-T
Kontext	27.48	8.50	0.62	6.51	90.74	26.35
Kontext + Ours	27.54	8.62	0.62	6.53	91.67	26.41

diffusion models for image and video generation. Following DiT, Multimodal Diffusion Transformers (MMDiTs) (Esser et al., 2024; Labs, 2024; Wu et al., 2025) facilitate text-image interactions through a unified transformer. Subsequent works (Team, 2025; Gong et al., 2025; OpenAI, 2024; Wan et al., 2025; Wang et al., 2026; Zhang et al., 2025) have promoted AI generated content (AIGC).

Improving cross-modal interactions in diffusion models. Early works (Rombach et al., 2022; Team, 2024b) inject text features into diffusion models via cross-attention mechanisms. DiT (Peebles & Xie, 2023; Chen et al., 2024) proposed adaLN-zero strategy to modulate textual features into diffusion transformers. MMDiTs (Esser et al., 2024; Labs, 2024; Wu et al., 2025) suggest that text and image features should be treated equally by jointly modeling them in a unified transformer architecture. Other paradigms include in-context conditioning (Huang et al., 2024) and auxiliary controlnets (Zhang et al., 2023; Mou et al., 2024). However, these methods do not dive deep into the DiT and only provide coarse adjusting strategies.

Understanding cross-modal interactions in diffusion models. Some works (Hertz et al., 2022; Cao et al., 2023; Liu et al., 2024) investigate the role of attention mechanisms in Unet-based diffusion models for instruction-based editing. They reveal that attention values largely reflect the intensity of text-image interactions. Classifier-free guidance (CFG) (Ho & Salimans, 2022) adopts a static scaling

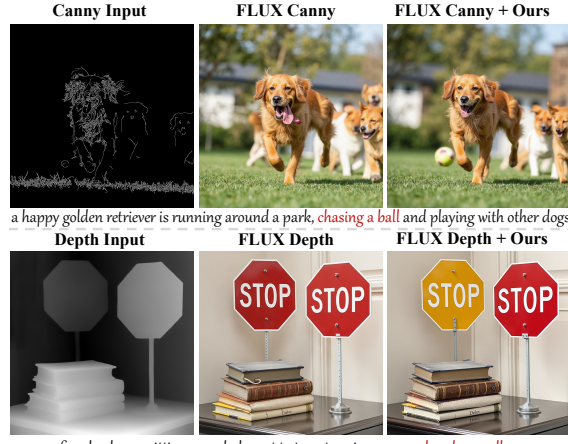


Figure 7. Qualitative results of integrating *Diff-Aid* with controllable modules. Our method can be integrated into controllable generation for enhanced interactions of textual conditions.

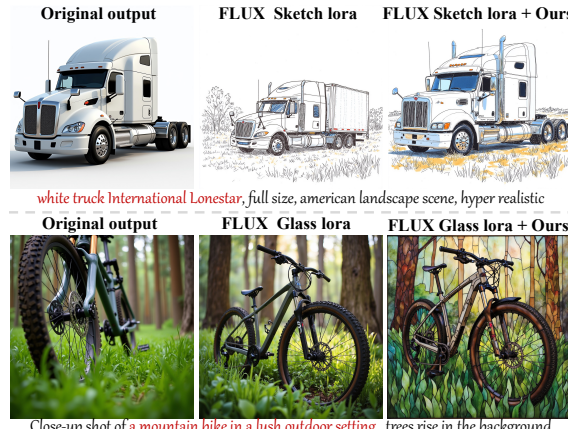


Figure 8. Qualitative results of combining *Diff-Aid* with off-the-shelf LoRAs from the community. Our method can also be seamlessly combined with various style-based LoRAs for producing style images with quality.

factor to balance conditional and unconditional model outputs, thereby controlling textual strength. Despite these advances, a holistic understanding of DiT remains underexplored. TACA (Lv et al., 2025) identified cross-modal attention imbalance and introduced a time-aware weighting scheme. Li et al. (2026) dissected the block contributions and proposed block-wise conditioning strategies. However, no current method offers a unified perspective from block-wise, timestep-aware, and token-level viewpoints on how all components jointly influence generation quality.

5. Conclusion

We presented *Diff-Aid*, a plug-in module for rectified text-to-image diffusion transformers that learns to adaptively adjust block-wise interactions between token-level textual conditions across denoising trajectories. Beyond improving the generation quality, *Diff-Aid* provides insights into the dynamic interplay of cross-modal signals in transformer

blocks and can be seamlessly applied to various tasks.

Limitation and future work. Our current work focuses on rectified text-to-image generation, which may not directly extend to other modalities such as text-to-video or text-to-3D generation. Future work includes exploring the applicability of *Diff-Aid* to these modalities.

Impact Statement This work aims to improve diffusion models for text-to-image generation, with potential applications in creative fields like design and content creation. While these advancements could have broad societal benefits, ethical considerations around misuse, privacy, and copyright should be addressed in future work.

References

Alaluf, Y., Garibi, D., Patashnik, O., Averbuch-Elor, H., and Cohen-Or, D. Cross-image attention for zero-shot appearance transfer. In *ACM SIGGRAPH*, pp. 1–12, 2024.

Black Forest Labs, Batifol, S., Blattmann, A., Boesel, F., Consul, S., Diagne, C., Dockhorn, T., English, J., English, Z., Esser, P., et al. Flux. 1 kontext: Flow matching for in-context image generation and editing in latent space. *arXiv preprint arXiv:2506.15742*, 2025.

Cao, M., Wang, X., Qi, Z., Shan, Y., Qie, X., and Zheng, Y. Masactrl: Tuning-free mutual self-attention control for consistent image synthesis and editing. In *Int. Conf. Comput. Vis.*, pp. 22560–22570, 2023.

Chen, J., Yu, J., Ge, C., Yao, L., Xie, E., Wang, Z., Kwok, J. T., Luo, P., Lu, H., and Li, Z. Pixart- α : Fast training of diffusion transformer for photorealistic text-to-image synthesis. In *Int. Conf. Learn. Represent.*, 2024.

Dhariwal, P. and Nichol, A. Diffusion models beat gans on image synthesis. In *Adv. Neural Inform. Process. Syst.*, volume 34, pp. 8780–8794, 2021.

Esser, P., Kulal, S., Blattmann, A., Entezari, R., Müller, J., Saini, H., Levi, Y., Lorenz, D., Sauer, A., Boesel, F., et al. Scaling rectified flow transformers for high-resolution image synthesis. In *Int. Conf. Mach. Learn.*, 2024.

Ghosh, D., Hajishirzi, H., and Schmidt, L. Geneval: An object-focused framework for evaluating text-to-image alignment. In *Adv. Neural Inform. Process. Syst.*, volume 36, pp. 52132–52152, 2023.

Gong, L., Hou, X., Li, F., Li, L., Lian, X., Liu, F., Liu, L., Liu, W., Lu, W., Shi, Y., et al. Seedream 2.0: A native chinese-english bilingual image generation foundation model. *arXiv preprint arXiv:2503.07703*, 2025.

Han, J., Liu, J., Jiang, Y., Yan, B., Zhang, Y., Yuan, Z., Peng, B., and Liu, X. Infinity: Scaling bitwise autoregressive modeling for high-resolution image synthesis. In *IEEE Conf. Comput. Vis. Pattern Recog.*, pp. 15733–15744, 2025.

Hertz, A., Mokady, R., Tenenbaum, J., Aberman, K., Pritch, Y., and Cohen-Or, D. Prompt-to-prompt image editing with cross attention control. *arXiv preprint arXiv:2208.01626*, 2022.

Ho, J. and Salimans, T. Classifier-free diffusion guidance. *arXiv preprint arXiv:2207.12598*, 2022.

Ho, J., Jain, A., and Abbeel, P. Denoising diffusion probabilistic models. In *Adv. Neural Inform. Process. Syst.*, pp. 6840–6851, 2020.

Hu, E. J., Shen, Y., Wallis, P., Allen-Zhu, Z., Li, Y., Wang, S., Wang, L., Chen, W., et al. Lora: Low-rank adaptation of large language models. *Int. Conf. Learn. Represent.*, 1 (2):3, 2022.

Huang, L., Wang, W., Wu, Z.-F., Shi, Y., Dou, H., Liang, C., Feng, Y., Liu, Y., and Zhou, J. In-context lora for diffusion transformers. *arXiv preprint arXiv:2410.23775*, 2024.

Karras, T., Aittala, M., Aila, T., and Laine, S. Elucidating the design space of diffusion-based generative models. *Adv. Neural Inform. Process. Syst.*, 35:26565–26577, 2022.

Labs, B. F. Flux. github.com/black-forest-labs/flux, 2024.

Li, B., Yang, M., Tan, Z., Zhang, J., and Li, H. Unraveling mmdit blocks: Training-free analysis and enhancement of text-conditioned diffusion. *arXiv preprint arXiv:2601.02211*, 2026.

Lin, H., Chen, Y., Wang, J., An, W., Wang, M., Tian, F., Liu, Y., Dai, G., Wang, J., and Wang, Q. Schedule your edit: A simple yet effective diffusion noise schedule for image editing. *Adv. Neural Inform. Process. Syst.*, 37: 115712–115756, 2024.

Liu, B., Wang, C., Cao, T., Jia, K., and Huang, J. Towards understanding cross and self-attention in stable diffusion for text-guided image editing. In *IEEE Conf. Comput. Vis. Pattern Recog.*, pp. 7817–7826, 2024.

Liu, X., Gong, C., et al. Flow straight and fast: Learning to generate and transfer data with rectified flow. In *Int. Conf. Learn. Represent.*, 2023.

Lv, Z., Pan, T., Si, C., Chen, Z., Zuo, W., Liu, Z., and Wong, K.-Y. K. Rethinking cross-modal interaction in multimodal diffusion transformers. In *Int. Conf. Comput. Vis.*, 2025.

Ma, X., Wang, Y., Jia, G., Chen, X., Liu, Z., Li, Y.-F., Chen, C., and Qiao, Y. Latte: Latent diffusion transformer for video generation. *arXiv preprint arXiv:2401.03048*, 2024.

Ma, Y., Wu, X., Sun, K., and Li, H. Hpsv3: Towards wide-spectrum human preference score. In *Int. Conf. Comput. Vis.*, 2025.

Mishchenko, K. and Defazio, A. Prodigy: An expeditiously adaptive parameter-free learner. In *Int. Conf. Mach. Learn.*, 2024.

Mou, C., Wang, X., Xie, L., Wu, Y., Zhang, J., Qi, Z., and Shan, Y. T2i-adapter: Learning adapters to dig out more controllable ability for text-to-image diffusion models. In *Assoc. Adv. Artif. Intell.*, volume 38, pp. 4296–4304, 2024.

OpenAI. Video generation models as world simulators. 2024. Technical Report, OpenAI.

Peebles, W. and Xie, S. Scalable diffusion models with transformers. In *IEEE Conf. Comput. Vis. Pattern Recog.*, pp. 4195–4205, 2023.

Qiu, Z., Wang, Z., Zheng, B., Huang, Z., Wen, K., Yang, S., Men, R., Yu, L., Huang, F., Huang, S., et al. Gated attention for large language models: Non-linearity, sparsity, and attention-sink-free. *Adv. Neural Inform. Process. Syst.*, 2025.

Radford, A., Kim, J. W., Hallacy, C., Ramesh, A., Goh, G., Agarwal, S., Sastry, G., Askell, A., Mishkin, P., Clark, J., et al. Learning transferable visual models from natural language supervision. In *Int. Conf. Mach. Learn.*, pp. 8748–8763, 2021.

Rombach, R., Blattmann, A., Lorenz, D., Esser, P., and Ommer, B. High-resolution image synthesis with latent diffusion models. In *IEEE Conf. Comput. Vis. Pattern Recog.*, pp. 10684–10695, 2022.

Schuhmann, C. Laion aesthetics. github.com/LAION-AI/aesthetic-predictor, 2022.

Song, J., Meng, C., and Ermon, S. Denoising diffusion implicit models. In *Int. Conf. Learn. Represent.*, 2021.

Stability-AI. Stable diffusion 3.5. github.com/Stability-AI/sd3.5, 2024.

Team, H. F. M. Hunyuanvideo: A systematic framework for large video generative models, 2024a. URL <https://github.com/Tencent-Hunyuan/HunyuanVideo>.

Team, H. F. M. Hunyuanimage-2.1: An efficient diffusion model for high-resolution (2k) text-to-image generation, 2025. URL <https://github.com/Tencent-Hunyuan/HunyuanImage-2.1>.

Team, K. Kolors: Effective training of diffusion model for photorealistic text-to-image synthesis. github.com/Kwai-Kolors/Kolors, 2024b.

Vaswani, A., Shazeer, N., Parmar, N., Uszkoreit, J., Jones, L., Gomez, A. N., Kaiser, Ł., and Polosukhin, I. Attention is all you need. *Adv. Neural Inform. Process. Syst.*, 30, 2017.

Wallace, B., Dang, M., Rafailov, R., Zhou, L., Lou, A., Purushwalkam, S., Ermon, S., Xiong, C., Joty, S., and Naik, N. Diffusion model alignment using direct preference optimization. In *IEEE Conf. Comput. Vis. Pattern Recog.*, pp. 8228–8238, 2024.

Wan, T., Wang, A., Ai, B., Wen, B., Mao, C., Xie, C.-W., Chen, D., Yu, F., Zhao, H., Yang, J., et al. Wan: Open and advanced large-scale video generative models. *arXiv preprint arXiv:2503.20314*, 2025.

Wang, J., Qiang, C., Guo, Y., Wang, Y., Zeng, X., Zhang, C., and Wan, P. Klear: Unified multi-task audio-video joint generation. *arXiv preprint arXiv:2601.04151*, 2026.

Wu, C., Li, J., Zhou, J., Lin, J., Gao, K., Yan, K., Yin, S.-m., Bai, S., Xu, X., Chen, Y., et al. Qwen-image technical report. *arXiv preprint arXiv:2508.02324*, 2025.

Wu, X., Hao, Y., Sun, K., Chen, Y., Zhu, F., Zhao, R., and Li, H. Human preference score v2: A solid benchmark for evaluating human preferences of text-to-image synthesis. *arXiv preprint arXiv:2306.09341*, 2023.

Xu, J., Liu, X., Wu, Y., Tong, Y., Li, Q., Ding, M., Tang, J., and Dong, Y. Imagereward: learning and evaluating human preferences for text-to-image generation. In *Adv. Neural Inform. Process. Syst.*, pp. 15903–15935, 2023.

Yang, Z., Teng, J., Zheng, W., Ding, M., Huang, S., Xu, J., Yang, Y., Hong, W., Zhang, X., Feng, G., et al. Cogvideox: Text-to-video diffusion models with an expert transformer. In *Int. Conf. Learn. Represent.*, 2025.

Zhang, G., Zhou, Z., Hu, T., Peng, Z., Zhang, Y., Chen, Y., Zhou, Y., Lu, Q., and Wang, L. Uniavgen: Unified audio and video generation with asymmetric cross-modal interactions. *arXiv preprint arXiv:2511.03334*, 2025.

Zhang, L., Rao, A., and Agrawala, M. Adding conditional control to text-to-image diffusion models. In *Int. Conf. Comput. Vis.*, pp. 3836–3847, 2023.

A. Outline of Appendix

We provide additional details and results to supplement the main paper as follows. We first present more details about our experimental setup in Sec. B, including baselines, evaluation metrics, datasets, and implementation details of optimization choices. Then, in Sec. C, we raise a sparse enhancement strategy based on our learned α values. Quantitative and qualitative results are provided. Next, we provide more quantitative results in Sec. D, including quantitative results on applications, analysis of the heatmap of α values, distribution of α across different timesteps, and more ablation of dropout probability. Finally, the Sec. E provides additional qualitative results and failure cases.

B. Details of Experimental Setup

B.1. Details of Baselines

We conduct experiments on two strong text-to-image diffusion models: Stable Diffusion 3.5 Large (SD 3.5) ([Stability-AI, 2024](#)) and FLUX.1-Dev ([Labs, 2024](#)). We use the official checkpoints provided by the authors and do not perform any fine-tuning on these models. During inference, model weights are loaded in 16-bit precision. No acceleration techniques such as xformers or memory-efficient attention are used. The Tab. 5 summarizes the key hyperparameters used during inference for both models.

Table 5. Default inference hyper-parameters for both SD 3.5 and FLUX.

Model	DiT Blocks	Parameters	Inference Timesteps	Sampler	CFG Scale	Image Size
SD 3.5	38	8B	28	EDM	7.0	1024×1024
FLUX	57	12B	28	EDM	3.5	1024×1024

B.2. Details of Evaluation Metrics

To comprehensively evaluate the performance of our proposed method, we utilize a suite of established evaluation metrics that assess various aspects of text-to-image generation quality, including prompt adherence, image quality, and semantic alignment. We employ the following evaluation metrics to assess the performance of our proposed method.

- **HPSv2** ([Wu et al., 2023](#)) can effectively evaluate the preference score of text-image pairs or multiple images given a text prompt. It is trained on a large-scale human preference dataset and has shown strong correlation with human judgments.
- **HPSv3** ([Ma et al., 2025](#)) is derived from the QWen2-VL and trained on the HPDv3 dataset. It demonstrates improved performance over HPSv2 in evaluating text-image alignment and image quality.
- **ImageReward** ([Xu et al., 2023](#)) utilizes preference data collected from human feedback and applies reinforcement learning to train a reward model that can evaluate the image preference score and provide feedback in reward signals.
- **Aesthetic Score** ([Schuhmann, 2022](#)) primarily focuses on assessing the overall aesthetic quality of an image, which is built upon the CLIP models. This score is often subjective regarding composition, color harmony, and visual appearance.
- **Geneval Score** ([Ghosh et al., 2023](#)) propose an object-focused evaluation metric for text-to-image generation models. It defines a set of tasks to evaluate different aspects of text-image alignment, including “Single Object”, “Two Object”, “Counting”, “Position”, and “Attribute binding”. The Geneval Score is computed as the average accuracy across these tasks. It primarily focused on evaluating the model’s ability for semantic alignment.
- **CLIP Score** ([Radford et al., 2021](#)) measures the cosine similarity between the image and text embeddings obtained from a pre-trained CLIP model. CLIP-I and CLIP-T are used to evaluate the editing tasks.



Figure 9. Results of sparse enhancement strategy compared to the full method and baseline FLUX. Our sparse enhancement achieves similar performance as the full method, showing the effectiveness of our learned α values in identifying important blocks for text-image interactions. The hpsv3 scores, image reward scores, and aesthetic scores are provided at the bottom of each image for reference.

B.3. Details of Datasets

Training Datasets. HPDv3 dataset (Ma et al., 2025) totally contains 1.17 million binary preference choices over 1.08 million images, grouped in pairs by prompts. These images are collected from various sources, including real images, MidJourney, Cogview4, FLUX, HunyuanDiT, Stable Diffusion 3 Medium, Stable Diffusion 1.4, and Glide, etc. Most sources are not competitive text-to-image models with FLUX and SD 3.5, which use all the images from suboptimal models, which may lead to inferior performance.

To ensure the training data quality, we filter the HPDv3 dataset using the following criteria: 1) Preference confidence filter. We only keep the image pairs with preference confidence scores higher than 0.9. 2) Image quality filter. We only keep the image pairs where the preferred images are from real images, FLUX, or Kolors. After filtering, we obtain 77,252 image pairs for training our *Aid* on both baselines.

Subset of HPDv3 Benchmark. HPDv3 benchmark consists of 12,000 prompts covering a wide range of categories, including “Animals”, “Architecture”, “Arts”, “Characters”, “Design”, “Food”, “Nature Scenery”, “Plants”, “Products”, “Science”, “Transportation”, and “Others”. Each category contains 1,000 prompts. Tab. 1, 2 in the main paper report the results on the whole HPDv3 benchmark. Other than the full benchmark, we also report the results on the 20% subset of HPDv3 in Tab. 3 and 8, which contains 2,400 prompts sampled from all categories.

B.4. Details of optimization choices

In Sec. 2.2 of the main paper, we introduce several optimization choices to enhance the training stability and performance of our *Aid*. In ablation studies (Tab. 3), we systematically evaluate the impact of four different optimization choices. Here, we provide more implementation details for each choice.

1) LoRA + SFT. We apply LoRA (Hu et al., 2022) with a rank of 64 to all the linear layers in the FLUX. No *Aid* is applied to the transformer blocks in this setting.

2) LoRA + DPO. Based on the LoRA setting above, we further apply DPO to optimize the parameters to obtain better performance. We set the DPO temperature β to 0.1 and use the original FLUX as the reference model. The λ_{dpo} is set to 1.0, which is commonly used in previous works (Wallace et al., 2024).

3) Ours + Rwd. In this setting, we use all the designs in our *Aid*, including Tanh activation, α regularization ($\lambda_{reg} = 0.1$), gated mechanism, and skipping during training ($p = 0.1$). The *Aid* has an “mlp_hidden_dim” of 2048. We further incorporate

the HPSv3 as the reward model to provide additional reward signals during training. The reward weight λ_{rwd} is set to 1.0. To keep the reward scores in a reasonable range, we only apply reward learning when the timestep t is smaller than 0.3.

4) Ours + DPO. Similar to the settings of “Ours + Rwd”, we use all the designs in our *Aid*. We further apply DPO to optimize the parameters. The DPO settings are the same as those in “LoRA + DPO”.

In Tab. 3, we can observe that the giant leap in performance mainly comes from our *Aid* designs and sparsity strategies. Incorporating additional optimization strategies like DPO can further boost the performance. Therefore, our default settings are using all the designs in our *Aid* block and applying DPO for optimization.

C. Sparse Enhancement Results

Li et al. (2026) selected a subset of transformer blocks in MMDiT to enhance the text embeddings. This approach depends on the prior knowledge of which blocks are vital for text-image generation. From Fig. 4(a) in the main paper, we can observe that some blocks have higher α values, indicating their importance in text-image interactions. We simply select the blocks $\{1, 15, 36, 41, 48\}$ for FLUX and set the α to 0.5 for these blocks and 0.0 for others. This sparse enhancement strategy overlooks the learned timestep-awareness and token-level modulation in our *Aid*. However, it provides insights into the effectiveness of enhancing only a few crucial blocks. As shown in Fig. 9 and Tab. 6, our sparse enhancement strategy gets similar outputs as our full method. ImageReward score (0.98) of sparse enhancement even outperforms our full method. This indicates that enhancing only a few important blocks can already bring significant improvements. Quantitative and qualitative results demonstrate that our learned α values effectively identify crucial blocks for text-image interactions.

Table 6. Quantitative results of sparse enhancement strategy compared to the full method and baseline FLUX. Our sparse enhancement achieves suboptimal but competitive performance compared to the baseline. This indicates the effectiveness of our learned α values in identifying important blocks for text-image interactions.

Strategies	HPSv2	HPSv3	ImgRwd	Aes.
FLUX	28.53	10.42	0.89	6.66
Sparse Enhancement	<u>28.61</u>	<u>10.57</u>	0.98	<u>6.71</u>
Our Full Method	28.80	10.84	<u>0.95</u>	6.76

D. More Quantitative Results

D.1. Quantitative Results on Applications

In Sec. 3.5 of the main paper, we demonstrate the versatility of our proposed *Diff-Aid* by applying it to different conditional generation tasks. We visualize some qualitative results in Fig. 6, Fig. 7 and Fig. 8. Here, we further evaluate our method on two applications: 1) using “Canny”¹ and “Depth”² conditions. 2) using “Sketch”³ and “Glass”⁴ LoRA modules to adapt to new styles. The quantitative results are shown in Tab. 7.

Table 7. Quantitative results of applying our *Diff-Aid* to style LoRAs and control conditions generation. Our method can be flexibly applied to different applications while obtaining competitive performance improvements.

Strategies	HPSv2	HPSv3	ImgRwd	Aes.
LoRA	28.53	10.42	0.89	6.66
LoRA + Ours	28.54	10.43	0.86	6.63
Control	28.57	10.48	0.90	6.67
Control + Ours	28.76	10.68	0.93	6.70

These results are obtained on the FLUX model on the 20% of the HPDV3 dataset. Our method not only seamlessly integrates

¹<https://huggingface.co/black-forest-labs/FLUX.1-Canny-dev>

²<https://huggingface.co/black-forest-labs/FLUX.1-Depth-dev>

³<https://huggingface.co/Shakker-Labs/FLUX.1-dev-LoRA-Children-Simple-Sketch>

⁴<https://civitai.com/models/553811/stained-glass?modelVersionId=771546>

with these models but also significantly enhances their performance in terms of prompt adherence and image quality. This demonstrates the versatility and effectiveness of our approach across different conditional generation tasks.

D.2. Heatmap of Alpha Values

Fig. 4(a) and (b) in the main paper show the distribution of α values across various transformer blocks and timesteps, respectively. Here, Fig. 10 provides a more detailed visualization of each block's α values at different timesteps for both models. Actually, the sharp changes described in Fig. 4(c) of the main paper can also be observed in the attention heatmap in Fig. 10b, where some blocks (41st – 54th) exhibit significant variations in α values at the timestep 11. In this way, we can clearly see how our *Diff-Aid* dynamically adjusts the block-wise interactions between token-level textual conditions across different timesteps.

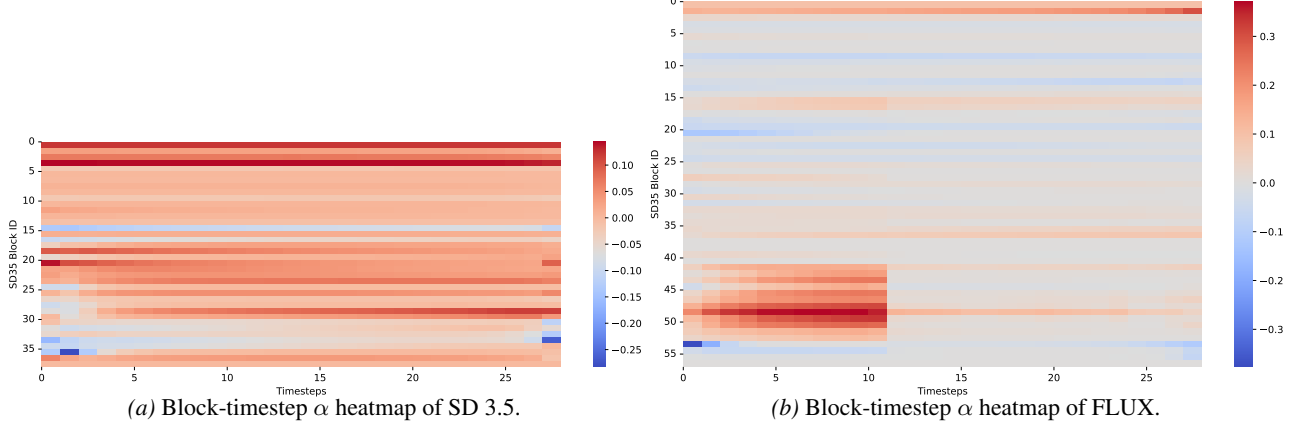


Figure 10. Visualization of the α across different timesteps and blocks for the models.

D.3. Distribution of α across different timesteps

In Fig. 4(c) of the main paper, we plot the distribution of α values across timesteps ($T = 28$) for both SD 3.5 and FLUX. Here, we further visualize the distribution of α values across different timesteps ($T \in \{6, 8, 10, 20, 28, 40, 50, 60\}$) for both models in Fig. 11. As shown in Fig. 11, the distributions of α values at different timesteps exhibit similar patterns and do not vary significantly with the number of sampling steps. As the timestep increases, the curve shows a stable convergence trend, indicating that the modulation ability of our *Diff-Aid* stabilizes at higher timesteps. This indicates that our *Aid* effectively captures the timestep-aware interactions between token-level textual conditions, maintaining consistent behavior across various sampling step configurations.

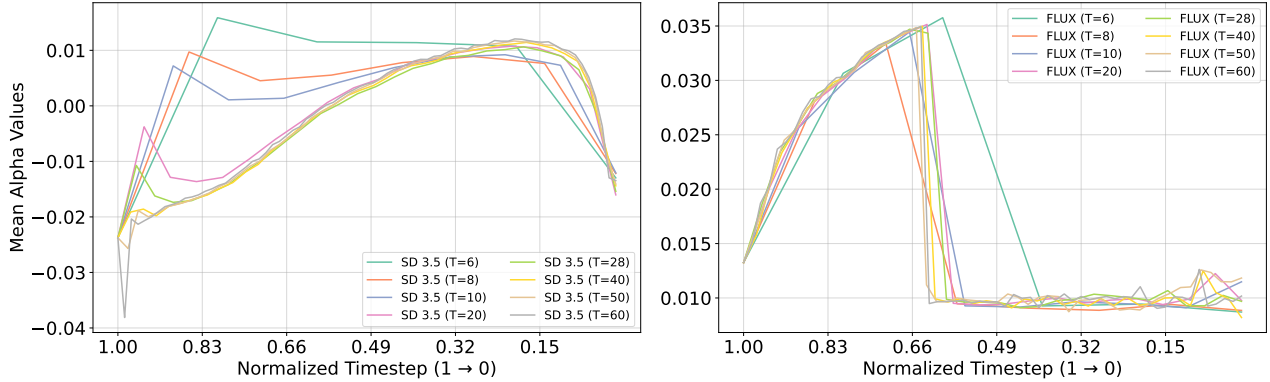


Figure 11. Distribution of α values across different timesteps for both SD 3.5 and FLUX. The distributions of α values at different timesteps exhibit similar patterns and do not vary significantly with the number of sampling steps.

D.4. More Ablation of dropout probability.

We further investigate the impact of different dropout probabilities in our *Aid* on the performance of FLUX. As shown in Tab. 8, we experiment with dropout probabilities ranging from 0.0 to 0.7. The results indicate that a dropout probability of 0.1 yields the best performance across all metrics. When the dropout probability grows to 0.2, the performance slightly decreases but remains competitive. Big probabilities like 0.5 and 0.7 lead to significant drops in all metrics. These results suggest that incorporating a small amount of dropout helps regularize the model, preventing overfitting while still allowing it to learn effective modulation patterns. In contrast, big p values may cause excessive information loss during training and inference mismatch, leading to degraded performance.

Table 8. More ablation studies on different dropout probabilities.

Categories	Settings	HPSv2	HPSv3	ImgRwd	Aes.
FLUX		28.53	10.42	0.89	6.66
Dropout Probability	$p=0.0$	28.71	10.74	<u>0.94</u>	6.72
	$p=0.1$	28.80	10.84	0.95	6.76
	$p=0.2$	28.73	10.77	0.94	6.73
	$p=0.3$	28.47	10.44	0.87	6.64
	$p=0.5$	28.21	10.19	0.77	6.59
	$p=0.7$	27.03	9.42	0.35	6.54

E. More Qualitative Results

E.1. More Results on FLUX and SD 3.5

In the following Fig. 12 and Fig. 13, we provide more qualitative comparisons of images generated by baseline FLUX and SD 3.5 with and without our proposed *Diff-Aid*. The quantitative results below each image show the scores of HPSv3, Image Reward, and Aesthetic Score. Our method demonstrates superior prompt adherence and image quality.

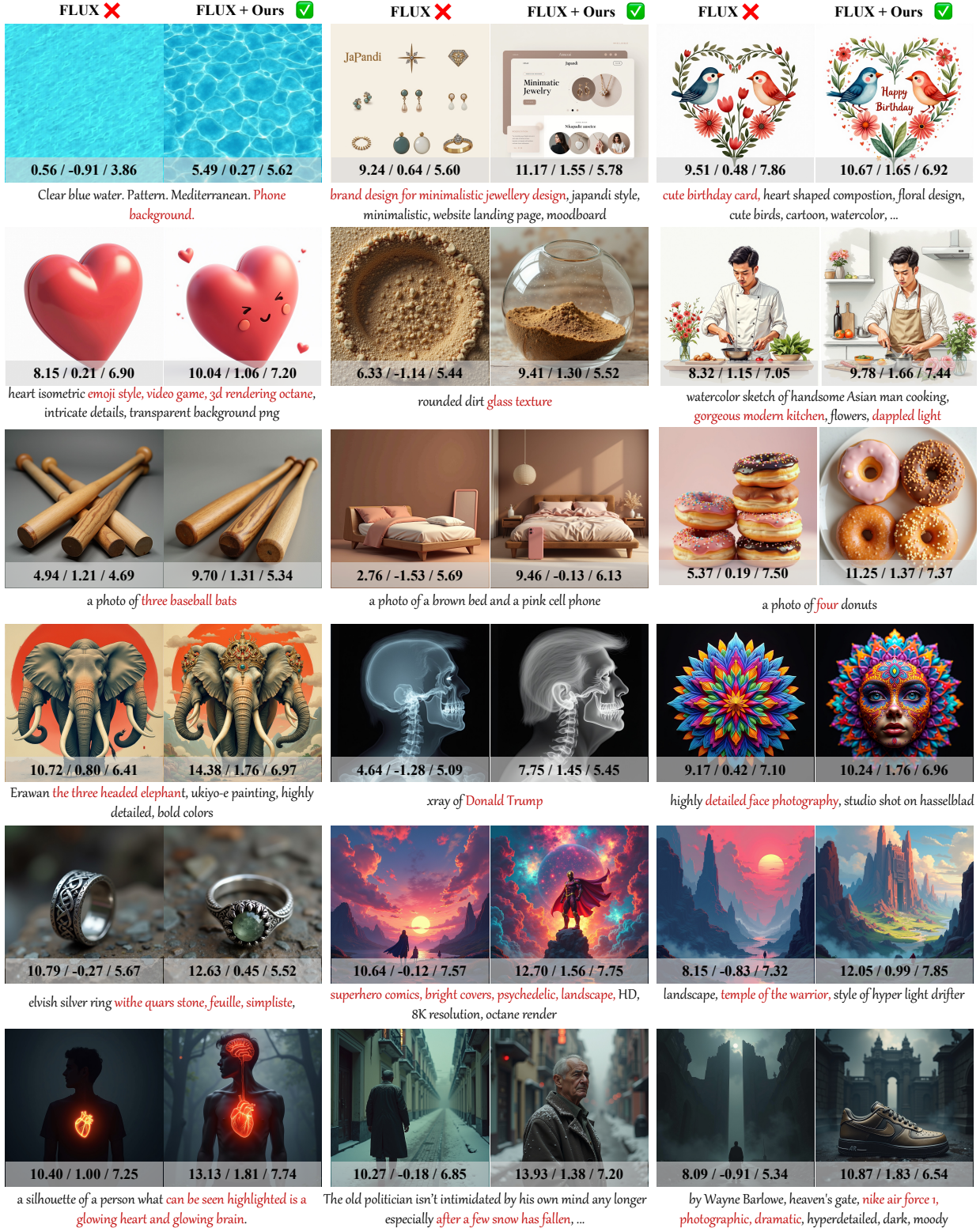


Figure 12. More Qualitative comparisons of images generated by baseline FLUX with and without our proposed Diff-Aid. The quantitative results below each image show the scores of HPSv3, Image Reward, and Aesthetic Score. Our method demonstrates superior prompt adherence and image quality.

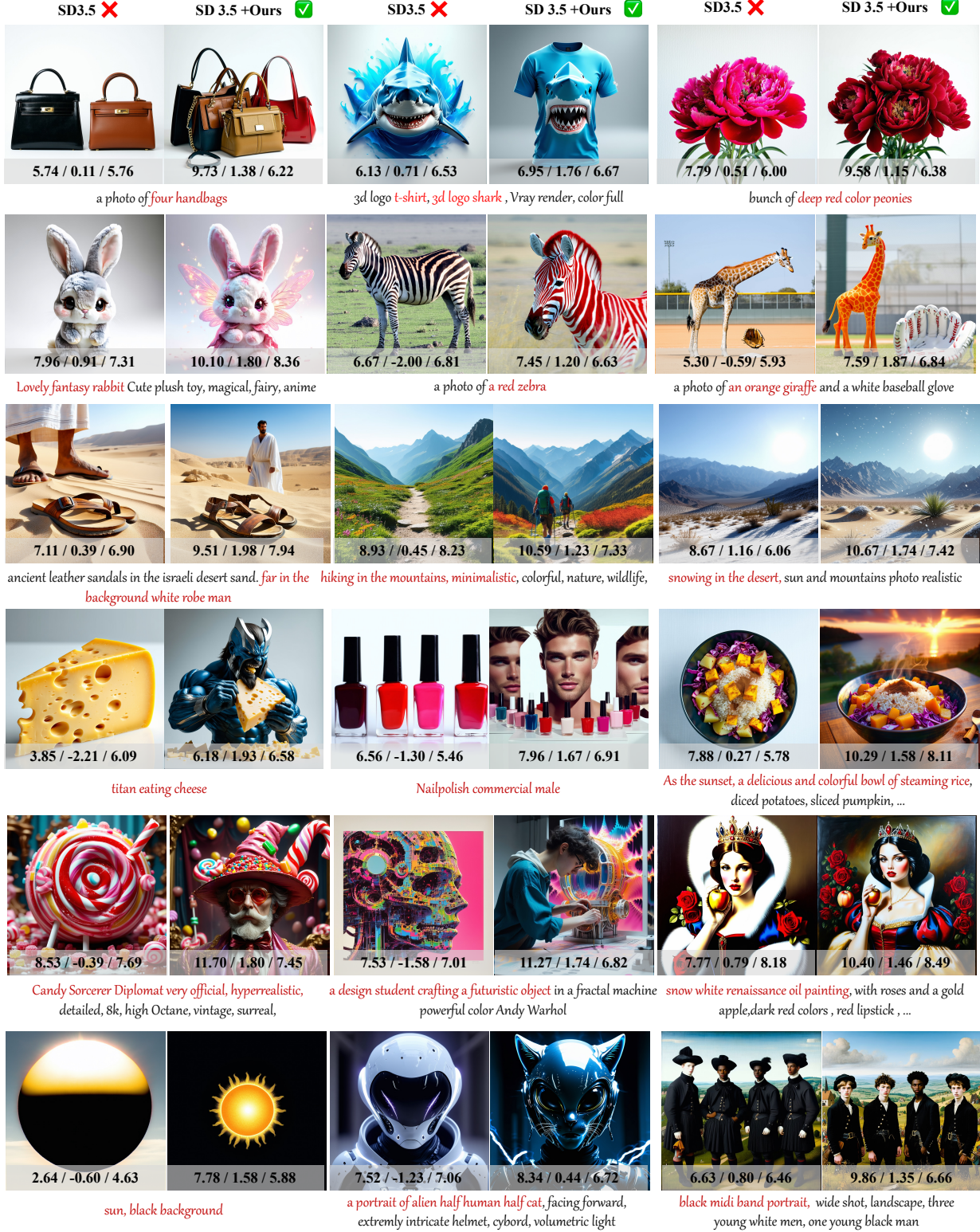


Figure 13. More Qualitative comparisons of images generated by baseline SD 3.5 with and without our proposed *Diff-Aid*. The quantitative results below each image show the scores of HPSv3, Image Reward, and Aesthetic Score. Our method demonstrates superior prompt adherence and image quality.

E.2. Failure Cases

In Fig. 14, we present some failure cases where the generated images do not accurately reflect the given prompts, even with our *Diff-Aid*. However, FLUX with our *Diff-Aid* manages to capture certain elements, such as the presence of the “vase” (second row, first example), and the “dog and teddy bear” (first row, second example). SD 3.5 with our *Diff-Aid* captures the prompt details but gets the lower quality scores. Although our generated images do not fully comply with the prompts, they still contain some key elements mentioned in the prompts. This indicates that our *Diff-Aid* helps improve textual-visual alignment, even in challenging scenarios.

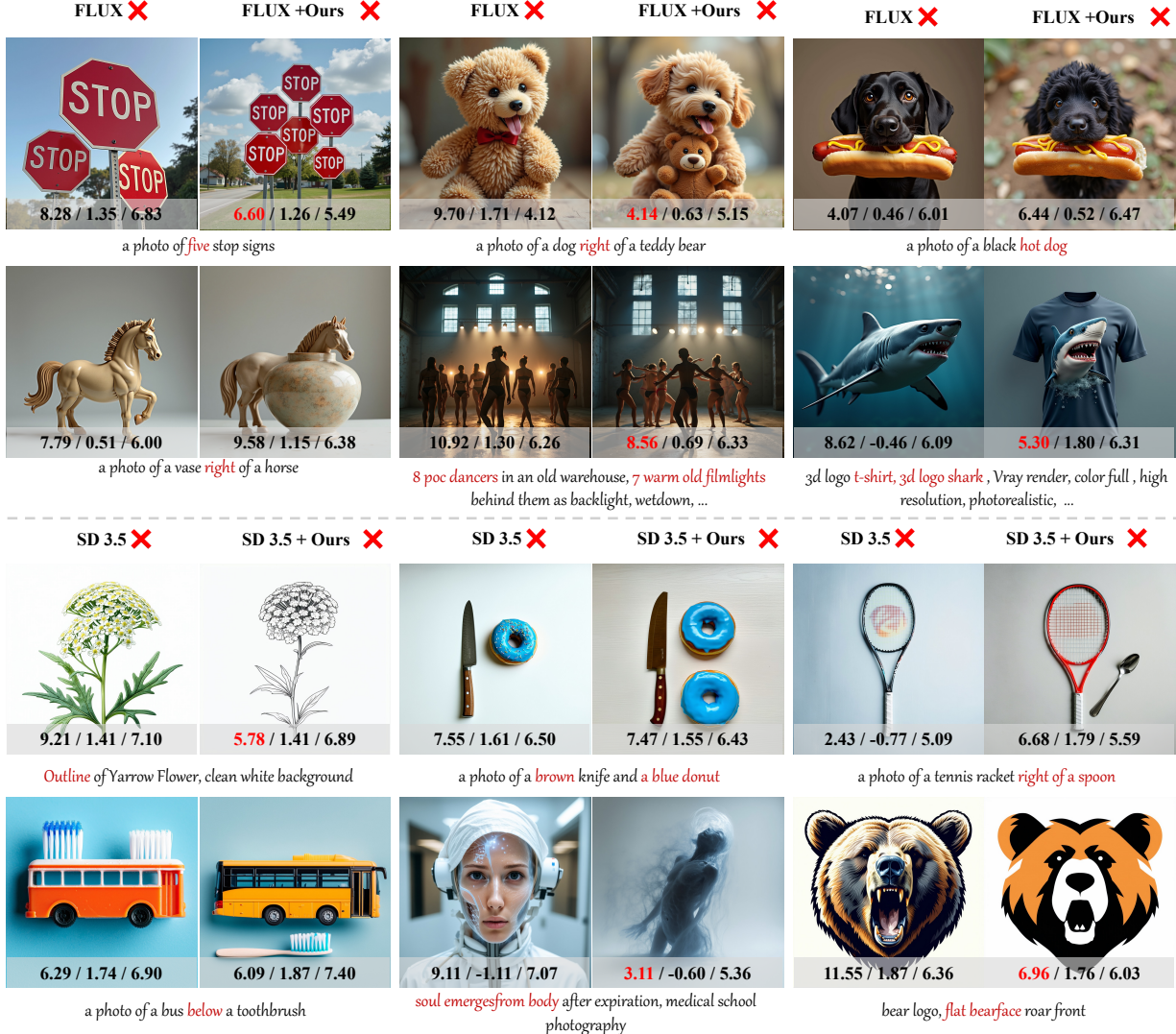


Figure 14. Some failure cases of baseline models with and without our proposed *Diff-Aid*. Although our generated images do not fully comply with the prompts, they still contain some key elements mentioned in the prompts.